Kinematic Modeling of a Flat-foldable Auxetic Metamaterial*

Huijuan Feng, Wujie Shi, Pino Trogu, and Jian S. Dai, *Fellow, IEEE*

Abstract— **Although many metamaterials can change shape, this flexibility often comes at the expense of the structural integrity which is difficult to preserve in their reconfigured mode. In this work, we introduce a transformable, flat-foldable shape designed in 1996 by the Italian topology researcher Giorgio Scarpa, consisting of a prismatic tetrahedron with additional hinges which bisect the walls of the extruded prisms. The shape is rigid when unfolded, and when scaled into a periodic, space-filling honeycomb, it yields a flat-foldable, prismatic metamaterial that preserves its developed, structurally sound unfolded state in the absence of external stimuli or mechanical loads. However, this new metamaterial is still kinematically rigid when only revolute hinges are admitted. To overcome the limitation that this improved design still relies on bending of the plates and torsional hinges, we introduce additional bisecting hinges along the diagonal of eight of the twenty-four square plates in the extruded tetrahedral unit cell. This modified design, now with only rigid plates and revolute hinges throughout the material, preserves both the rigidity and the flat-foldability, while also introducing the rigid foldability due to the presence of the additional diagonal hinges. A kinematic analysis of the folding motion of the tetrahedral unit cell is presented, showing how this bisecting technique can be generalized to yield auxetic metamaterials with both rigid foldability and negative Poisson's ratio. The straightforward bisecting of rigid plates connected by standard revolute hinges offers great opportunity for the design of reconfigurable metamaterials, mechanisms, and robots that combine flat-foldability and self-supported structural integrity when unfolded.**

I. Introduction

Metamaterials, thanks to their constitutive components or their structures, have unlocked desirable and exotic properties that conventional materials can't achieve. Origami metamaterials are a promising subset of metamaterials because of their superior folding properties [1-8]. "Auxetic" structures are artificially architected structures that exhibit negative Poisson's ratio [9]. That auxetic property enhances resistance to indentation at locations subject to concentrated loads. Auxeticity also increases resilience against shear deformation and enhances resistance to fracture [10]. In sum: Origami is an important conceptual paradigm for designing auxetic metamaterials [11, 12].

While many metamaterials can change shape and become reconfigurable, this adaptability often compromises their structural integrity, making it challenging to preserve their reconfigured state. Given that the majority of engineering materials utilized in constructing origami metamaterials tend to be relatively rigid, there is a particular focus on a subset of origami known as rigid origami [13, 14]. Rigid origami allows for seamless motion between folded and unfolded states along predetermined creases without any stretching or bending of the facets, making it particularly noteworthy. Dai and Jones pioneered a model for paper folding, assuming the creases to be revolute joints and the facets to be links [15-17]. This approach paved the way for analyzing rigid origami [18-21] from a mechanism perspective, as well as for the origami-based metamaterials [22, 23].

In 1996 the Italian researcher Giorgio Scarpa [24-27] invented a "transformable figure" consisting of a prismatic tetrahedron with additional hinges that bisect the walls of the extruded prisms [28]. When scaled periodically, this novel, previously unpublished design renders flat-foldable some rigid metamaterials such as "Material #1", introduced by Overvelde and others in 2017 and based on a tiling of tetrahedra and octahedra [29].

In this work, we introduce Scarpa's novel technique, in which the additional bisecting hinges applied to the prismatic walls of extruded polyhedra render these structures flat-foldable while preserving their rigidity. Scaled into space-filling honeycombs [30], these extruded polyhedra yield a new class of flat-foldable, prismatic metamaterials that preserve their developed, structurally sound, unfolded state in the absence of external stimuli or mechanical loads [31].

We found, however, that new metamaterials based on this bisecting technique would not be rigidly foldable since they would still rely on bending of the plates and torsional hinges [32, 33]. To resolve this limitation, we introduce additional bisecting hinges [34] along the diagonal of eight square plates in the extruded unit cell. This modified design, with additional diagonal hinges now contains only rigid plates and revolute hinges throughout. It preserves both rigidity and flat-foldability.

The layout is arranged as follows. In section 2, the rigid foldability and kinematic modeling of the original prismatic tetrahedron is conducted. Section 3 deals with the strategy of

*Research supported by the National Natural Science Foundation of China (Grant No. 52335003), the Guangdong Basic and Applied Basic Research Foundation (Grant No. 2023A1515110644), the Science, Technology, and Innovation Commission of Shenzhen Municipality under Grant ZDSYS20220527171403009 and JCYJ20220818100417038.

Research supported by a sabbatical award for the Academic Year 2017-2018, San Francisco State University (SFSU), and by Delft University of Technology (TU Delft, the Netherlands) for a visiting scholar sponsorship; by a Professional Development Council Grant, SFSU, AY 2018–2019; and by a Marcus Undergraduate Research Assistantship Grant, SFSU, AY 2023–2024.

H. Feng, W. Shi and J.S. Dai are with Shenzhen Key Laboratory of Intelligent Robotics and Flexible Manufacturing Systems, Southern University of Science and Technology, Shenzhen 518055, China (e-mail: fenghj@sustech.edu.cn; 12232287@mail.sustech.edu.cn; daijs@sustech.edu.cn).

P. Trogu is with the School of Design, San Francisco State University, San Francisco CA 94132 USA (corresponding author, phone: +1 415 627-7769; e-mail: trogu@sfsu.edu)

adding creases to the original prismatic tetrahedron to enable the rigid foldability and negative Poisson's ratio of the altered material. The kinematics of the altered vertices of the triangular prisms is conducted with the vector loop method in detail, followed by the compatibility analysis of the whole altered structure in section 4. Conclusions are outlined in section 5.

II. Rigid Foldability Analysis of Prismatic Tetrahedron with Kinematic Modeling

The original prismatic tetrahedron is formed by extruding four triangular prisms with additional bisecting creases from the tetrahedron as shown in Fig. 1. To analyze its rigid foldability, the ability to allow a structure to fold about crease lines without twisting or stretching component panels, a representative triangular prism with six vertices (*A*, *B*, *C*, *D*, *E*, *F*) is presented. It is found that central vertices *A*, *C* and *E* are composed of four creases while the corner vertices *B*, *D* and *F* are composed of six creases.

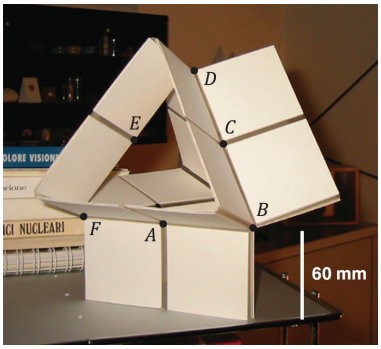

Figure 1. Original 1996 prismatic tetrahedron model with six representative vertices. Image courtesy of Giorgio Scarpa's archive, Castel Bolognese, Italy.

For the four-crease vertex, all of its rotational axes intersect at one point, so it can be modeled as a spherical 4*R* linkage and its closure equation can be established based on the Denavit and Hartenberg's (D-H) convention [35] as shown in Fig. 2. The z_i-axis is aligned with the *i*th joint axis, the x_i-axis is defined along the common normal between the (*i*-1)th and *i*th joint axes and points from the (*i*-1)th to the *i*th joint axis and the y_i-axis is determined by the right-hand rule, the geometric conditions for the spherical 4*R* linkage are

$$\alpha_{12} = \alpha_{23} = \alpha_{34} = \alpha_{41} = \frac{\pi}{2},$$
$$a_{12} = a_{23} = a_{34} = a_{41} = 0. \quad (1)$$

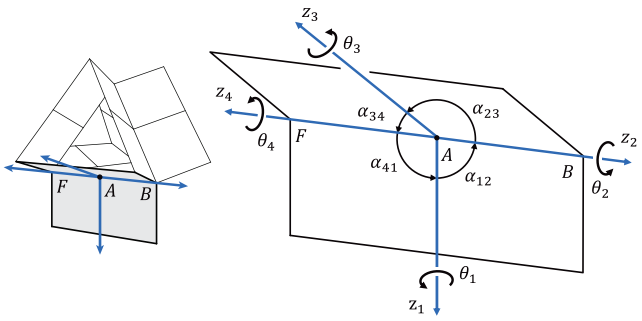

Figure 2. D-H notation of the four-crease vertex *A*.

The transformation matrix that transforms the expression in the (*i*+1)th coordinate system to the *i*th coordinate system is

$$\boldsymbol{Q}_{(i+1)i} = \begin{bmatrix} \cos\theta_i & -\cos\alpha_{i(i+1)}\sin\theta_i & \sin\alpha_{i(i+1)}\sin\theta_i \\ \sin\theta_i & \cos\alpha_{i(i+1)}\cos\theta_i & -\sin\alpha_{i(i+1)}\cos\theta_i \\ 0 & \sin\alpha_{i(i+1)} & \cos\alpha_{i(i+1)} \end{bmatrix} \quad (2)$$

and the inverse transformation is

$$\boldsymbol{Q}_{i(i+1)} = \begin{bmatrix} \cos\theta_i & \sin\theta_i & 0 \\ -\cos\alpha_{i(i+1)}\sin\theta_i & \cos\alpha_{i(i+1)}\cos\theta_i & \sin\alpha_{i(i+1)} \\ \sin\alpha_{i(i+1)}\sin\theta_i & -\sin\alpha_{i(i+1)}\cos\theta_i & \cos\alpha_{i(i+1)} \end{bmatrix} \quad (3)$$

According to the closure equation, the following formula can be obtained as

$$\boldsymbol{Q}_{21}\boldsymbol{Q}_{32} = \boldsymbol{Q}_{41}\boldsymbol{Q}_{34} \quad (4)$$

where $\boldsymbol{Q}_{21}$ and $\boldsymbol{Q}_{32}$ are obtained by replacing *i* in Eq. (2) with 1 and 2 respectively, while $\boldsymbol{Q}_{41}$ and $\boldsymbol{Q}_{34}$ are obtained by replacing *i* in Eq. (3) with 4 and 3 respectively, and *i*+1 is taken as 1 when $i = 4$. So the input-output relationship of the four-crease vertex is obtained as

$$\theta_1 = \theta_3 = 0,\ \theta_2 = \theta_4; \quad (5a)$$
$$\text{or } \theta_2 = \theta_4 = 0,\ \theta_1 = \theta_3. \quad (5b)$$

Considering the overall dihedral constraint of the extrusions, only Eq. (5a) holds in this structure, which means the joints 1 and 3 degenerate. A similar kinematic model holds for vertices *C* and *E*, so we have the triangular prism with only three active creases, i.e., creases *FB*, *BD* and *DF*, meaning that it is not rigidly foldable. So do the other three triangular prisms. Therefore, the whole structure is not rigidly foldable.

However, we can break the geometric constraints of the structure as shown in Fig. 3 to make the model flat foldable. In this case, there will be deformation along the creases, and the whole model performs as a non-rigid foldable structure.

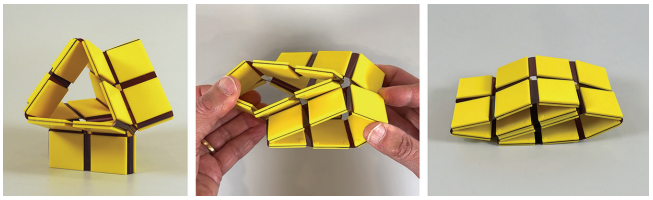

(a) (b) (c)

Figure 3. Non-rigid folding of prismatic tetrahedron: (a) Stable configuration; (b) Partially deformed configuration; (c) Flat-folded configuration.

III. Altered Rigidly Foldable Triangular Prism

A. Kinematics of the altered six-crease vertex

In order to make the whole structure rigidly foldable and to achieve the auxetic property, which means the whole structure squeezes in both directions with a negative Poisson's ratio, we add creases to the structure to increase its degrees of freedom (DoF). Considering the four-crease vertex in Fig. 2, we need to reactivate the degenerated joints 1 and 3. Therefore, we add two symmetric diagonal creases *AG* and *AH* to the four-crease vertex *A* as shown in Fig. 4.

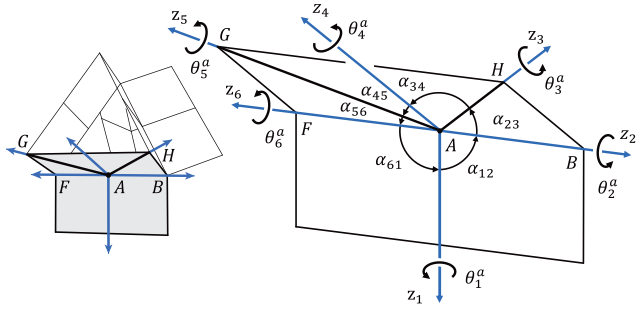

Figure 4. Altered vertex A with two additional symmetric creases.

The geometric conditions of the altered vertex are

$$\alpha_{12} = \alpha_{61} = \frac{\pi}{2}, \alpha_{23} = \alpha_{34} = \alpha_{45} = \alpha_{56} = \frac{\pi}{4}. \quad (6)$$

Considering the symmetric condition, the DoF of the altered crease is two, and we have

$$\theta_2^a = \theta_6^a,\ \theta_3^a = \theta_5^a. \quad (7)$$

The whole structure should be squeezed to achieve the auxetic property, so we fold the altered vertex A in Fig. 4 inward to analyze its motion. To better illustrate the vertex, the back view of Fig. 4 is taken as shown in Fig. 5(a). Assuming the input angles of the vertex are $\theta_1^a = \alpha_1$ and $\theta_2^a = \alpha_2$, the kinematics of the altered vertex can be solved with the vector loop method by calculating the angles θ_3^a and θ_4^a, which are the revolute angles along the creases AH and AP respectively. Since $AP \perp PH,\ AP \perp PG$, $\theta_4^a = \angle HPG$ and it can be figured out in ΔHPG using the cosine law, so we first need to calculate the vector $\boldsymbol{p}_4$.

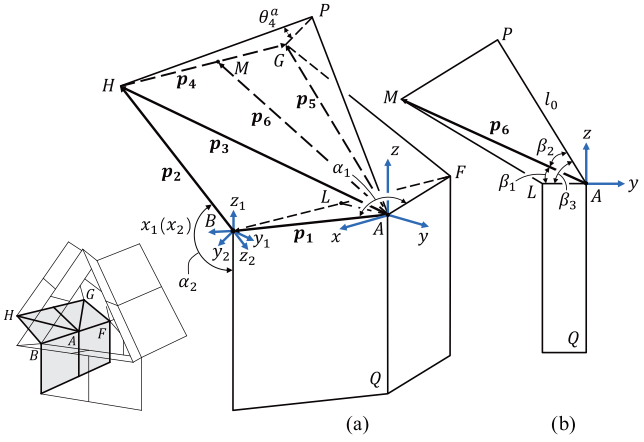

Figure 5. (a) Coordinate system setup and vector loop of the altered vertex; (b) Side view from the y-A-z plane.

Connect BF and HG and establish the coordinate systems $\{A\}$, $\{B_1\}$, $\{B_2\}$ as shown in Fig. 5(a), where the x-axis of the coordinate system $\{A\}$ is parallel with the line FB and its z-axis is colinear with QA, the x_1-axis of the coordinate system $\{B_1\}$ is along the line AB and its z_1-axis is parallel to QA, the x_2-axis of the coordinate system $\{B_2\}$ is along the line AB and its z_2-axis is along HB. The transformation from the coordinate system $\{A\}$ to the coordinate system $\{B_2\}$ can be decomposed into the following processes: a) translation along the x, y, z axes with the vector $\boldsymbol{p}_1$; b) rotation along the z_1 axis with the angle $-(\pi-\alpha_1)/2$; c) rotation along the x_1 axis with the angle $(2\pi-\alpha_2)$. Therefore, the vector $\boldsymbol{p}_3$ can be calculated by the coordinate transformation as

$$\overline{\boldsymbol{p}_3} = \overline{\boldsymbol{p}_H} = Trans(\boldsymbol{p}_1) \cdot Rot\left(z, \left(-\tfrac{\pi-\alpha_1}{2}\right)\right) \cdot Rot(x, (2\pi-\alpha_2)) \cdot \overline{\boldsymbol{p}_H^{B_2}} \quad (8)$$

where $\overline{\boldsymbol{p}_3}$ is the homogeneous coordinate of $\boldsymbol{p}_3$ in the coordinate system $\{A\}$, $\overline{\boldsymbol{p}_H}$ and $\overline{\boldsymbol{p}_H^{B_2}}$ are the homogeneous coordinates of point H represented in the coordinate systems $\{A\}$ and $\{B_2\}$ respectively. The vector $\boldsymbol{p}_1$ and $\boldsymbol{p}_H^{B_2}$ can be calculated as

$$\boldsymbol{p}_1 = \begin{bmatrix} l_0 \sin\frac{\alpha_1}{2} \\ -l_0 \cos\frac{\alpha_1}{2} \\ 0 \end{bmatrix},\ \boldsymbol{p}_H^{B_2} = \boldsymbol{p}_2^{B_2} = \begin{bmatrix} 0 \\ 0 \\ -l_0 \end{bmatrix} \quad (9)$$

where l_0 is the side length of the panel. So we have

$$\boldsymbol{p}_3 = \begin{bmatrix} l_0 \sin\frac{\alpha_1}{2} - l_0 \cos\frac{\alpha_1}{2} \sin\alpha_2 \\ -l_0 \cos\frac{\alpha_1}{2} - l_0 \sin\frac{\alpha_1}{2} \sin\alpha_2 \\ -l_0 \cos\alpha_2 \end{bmatrix} \quad (10)$$

Since $\boldsymbol{p}_3$ and $\boldsymbol{p}_5$ are symmetric about the y-A-z plane, the vector $\boldsymbol{p}_4$ can be calculated as

$$\boldsymbol{p}_4 = \boldsymbol{p}_5 - \boldsymbol{p}_3 = \begin{bmatrix} -2\left(l_0 \sin\frac{\alpha_1}{2} - l_0 \cos\frac{\alpha_1}{2} \sin\alpha_2\right) \\ 0 \\ 0 \end{bmatrix} \quad (11)$$

Therefore, the angle θ_4^a can be obtained by the cosine law

$$\cos\theta_4^a = \frac{\left|\overrightarrow{PH}\right|^2 + \left|\overrightarrow{PG}\right|^2 - |\boldsymbol{p}_4|^2}{2 \cdot \left|\overrightarrow{PH}\right| \cdot \left|\overrightarrow{PG}\right|} \quad (12)$$

where $\left|\overrightarrow{PH}\right| = \left|\overrightarrow{PG}\right| = l_0$, further we have

$$\theta_4^a = \arccos\left(1 - 2\left(\sin\frac{\alpha_1}{2} - \cos\frac{\alpha_1}{2} \sin\alpha_2\right)^2\right) \quad (13)$$

Then we need to figure out θ_3^a, which can be obtained by two normal vectors $\boldsymbol{n}_1$ and $\boldsymbol{n}_2$ of the plane AHB and AHP respectively. So we need to calculate the vector $\overrightarrow{AP}$ first, which requires the angle $\angle PAL$ known as shown in Fig. 5(a), where L is the midpoint of BF and AL is colinear with the y-axis. Taking the view from the y-A-z plane, the angle $\angle PAL = \beta_3$ is presented as shown in Fig. 5(b), where M is the midpoint of HG. So we have

$$\boldsymbol{p}_6 = \frac{1}{2}(\boldsymbol{p}_3 + \boldsymbol{p}_5) = \begin{bmatrix} 0 \\ -l_0 \cos\frac{\alpha_1}{2} - l_0 \sin\frac{\alpha_1}{2} \sin\alpha_2 \\ -l_0 \cos\alpha_2 \end{bmatrix} \quad (14)$$

And β_1 can be calculated as

$$\beta_1 = \arctan\left(-\frac{(\boldsymbol{p}_6)_z}{(\boldsymbol{p}_6)_y}\right) \quad (15)$$

where $(\boldsymbol{p}_6)_z$, $(\boldsymbol{p}_6)_y$ are the projection of $\boldsymbol{p}_6$ along the z and y axes respectively.

The angle β_2 can be obtained in the triangle $\Delta\, AMP$. Since $AP \perp PH, AP \perp PG$, AP is perpendicular to the plane HPG. MP is located in the plane HPG, so $MP \perp AP$. Then β_2 can be calculated as

$$\beta_2 = \arctan\left(\frac{|\overrightarrow{MP}|}{|\overrightarrow{AP}|}\right) \tag{16}$$

where $|\overrightarrow{MP}| = \sqrt{l_0^2 - \left(\frac{1}{2}|\boldsymbol{p}_4|\right)^2}$ and $|\overrightarrow{AP}| = l_0$.

So we have $\beta_3 = \beta_1 + \beta_2$ and

$$\overrightarrow{AP} = l_0 \cdot [0, \cos(\pi - \beta_3), \sin(\pi - \beta_3)]^T \tag{17}$$

Since the structure is folding inward where AH works as a mountain crease, θ_3^a is always larger than π during the folding process, then we can obtain

$$\theta_3^a = 2\pi - \arccos\left(\frac{\boldsymbol{n}_1 \cdot \boldsymbol{n}_2}{|\boldsymbol{n}_1| \cdot |\boldsymbol{n}_2|}\right) \tag{18}$$

where $\boldsymbol{n}_1 = \boldsymbol{p}_3 \times \boldsymbol{p}_1$ and $\boldsymbol{n}_2 = \boldsymbol{p}_3 \times \overrightarrow{AP}$. Eq. (18) can be simplified as

$$\theta_3^a = 2\pi - \arccos\left(\frac{\sigma_2\sigma_4\cos\sigma_3 - \sigma_1\sin\sigma_6\cos\alpha_2 + \sigma_4\cos\sigma_6\sin\sigma_3\cos\alpha_2}{\sqrt{|\sigma_2|^2 + |\cos\sigma_6\cos\alpha_2|^2 + |\sin\sigma_6\cos\alpha_2|^2}\sqrt{|\sigma_4\cos\sigma_3|^2 + |\sigma_4\sin\sigma_3|^2 + |\sigma_1|^2}}\right) \tag{19}$$

where

$\sigma_1 = \cos\sigma_3\cos\alpha_2 - \sigma_5\sin\sigma_3$

$\sigma_2 = \sigma_5\cos\sigma_6 - \sigma_4\sin\sigma_6$

$\sigma_3 = \arctan\left(\sqrt{1 - \left|\sin\frac{\alpha_1}{2} - \cos\frac{\alpha_1}{2}\sin\alpha_2\right|^2}\right) + \arctan\left(\frac{\cos\alpha_2}{\sigma_5}\right)$

$\sigma_4 = \cos\sigma_6 + \sin\sigma_6\sin\alpha_2$

$\sigma_5 = \sin\sigma_6 - \cos\sigma_6\sin\alpha_2$

$\sigma_6 = \frac{\alpha_1}{2} - \frac{\pi}{2}$.

Therefore, Eqs. (7), (13) and (19) form the whole set of kinematic equations for the altered vertex.

B. Kinematics of two triangular prisms with altered vertices

If we only change one vertex A while maintaining the other vertices for the triangular prism, as shown in Fig. 6(a), the whole structure will remain rigid since the two added creases will degenerate due to the other two fixed faces of the prism. It is observed from the motion of the physical model that there is deformation as well along the creases in the corner vertex. If we want to make the whole structure rigidly foldable, we also need to add creases along the corner vertex, so we altered the corner vertex as shown in Fig. 6(b).

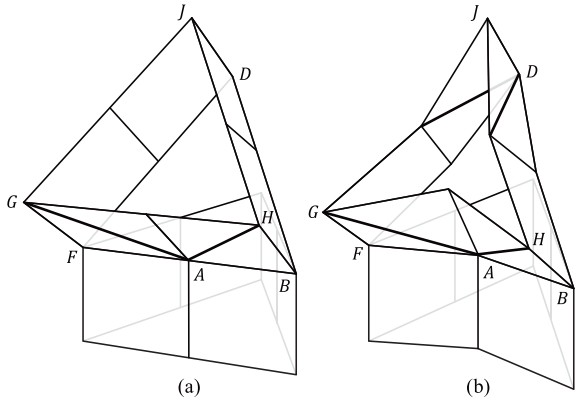

Figure 6. Double triangular prism group with (a) only one altered vertex A; (b) altered central vertex A and corner vertex D.

Since we only alter one central vertex A of the prism, the other four-crease vertices retain the original motion, meaning that the other two creases on the adjacent plane remain inactive, then we can draw Fig. 7 to calculate the kinematics of the altered triangular prism. It requires to find out angles $\theta_3^a, \theta_4^a, \theta_5^a, \theta_6^a, \theta_{11}, \theta_{12}, \theta_{13}, \theta_{14}, \theta_{21}, \theta_{22}, \theta_{23}$ with given α_1, α_2, where $\theta_3^a, \theta_4^a, \theta_5^a, \theta_6^a$ are rotational angles of vertex A, $\theta_{11}, \theta_{12}, \theta_{13}, \theta_{14}$ are rotational angles of the lower triangular prism and $\theta_{21}, \theta_{22}, \theta_{23}$ are defined in Fig. 7. Using the previous kinematics of the altered six-crease vertex, we can derive $\theta_3^a, \theta_4^a, \theta_5^a, \theta_6^a$ using Eqs. (7), (13) and (19) where $\theta_1^a = \alpha_1$, $\theta_2^a = \alpha_2$, then we only need to figure out $\theta_{11}, \theta_{12}, \theta_{13}, \theta_{14}, \theta_{21}, \theta_{22}, \theta_{23}$.

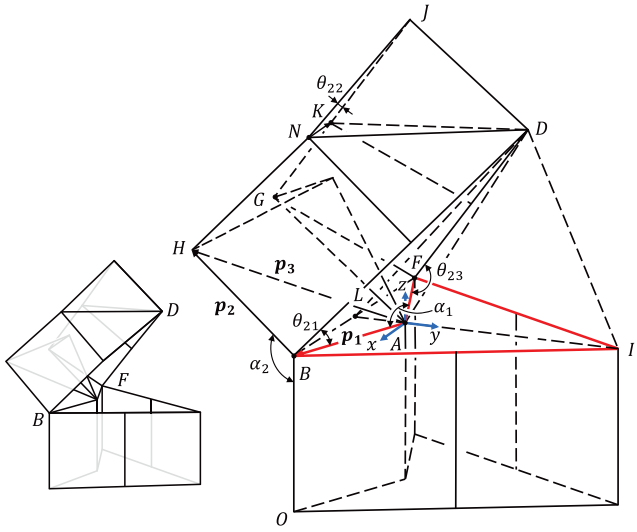

Figure 7. Schematic diagram of two triangular prisms with altered six-crease vertices.

Projecting the lower triangular prism along the line BO, we can obtain the projection in Fig. 8, where the six-panel mechanism degenerates to a planar four-bar linkage which only has one DoF.

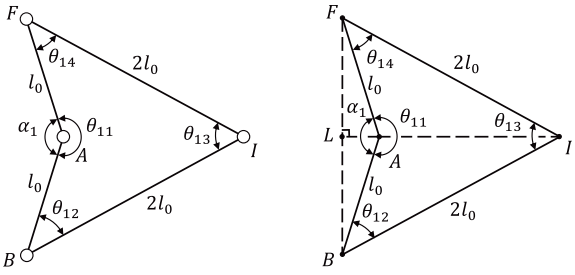

Figure 8. Projection of the lower triangular prism along the line BO.

As shown in Fig. 8, we have

$$\theta_{11} = 2\pi - \alpha_1 \tag{20}$$

According to the cosine law, we have

$$\cos\theta_{13} = \frac{(2l_0)^2 + (2l_0)^2 - |\overrightarrow{BF}|^2}{2\cdot(2l_0)\cdot(2l_0)} \tag{21}$$

where $|\overrightarrow{BF}|^2 = 2l_0^2 - 2l_0^2\cos\alpha_1$, so we have

$$\theta_{13} = \arccos\left(\frac{3}{4} + \frac{1}{4}\cos\alpha_1\right) \tag{22}$$

Since $|\overrightarrow{AF}| = |\overrightarrow{AB}| = l_0, |\overrightarrow{IF}| = |\overrightarrow{IB}| = 2l_0$, $\triangle AIF \cong \triangle AIB$, then

$$\theta_{12} = \theta_{14} = \pi - \frac{\theta_{11}}{2} - \frac{\theta_{13}}{2} = \frac{\alpha_1}{2} - \frac{\arccos\left(\frac{\cos\alpha_1}{4} + \frac{3}{4}\right)}{2} \tag{23}$$

The whole mechanism is symmetric about the *y*-*A*-*z* plane as shown in Fig. 8, so we have

$$\theta_{21} = \theta_{23} \tag{24}$$

In order to figure out θ_{21}, the vector $\overrightarrow{BD}$ should be calculated together with $\overrightarrow{AD}$. Since $HB \perp BA, HB \perp BD$; $GF \perp FA, GF \perp FD$; we have $HB \perp DA, GF \perp DA$, so

$$\overrightarrow{AD} = k_1 \cdot \overrightarrow{BH} \times \overrightarrow{FG} \tag{25}$$

where k_1 is a constant not equal to 0.

$$\overrightarrow{BH} = \boldsymbol{p}_2 = \boldsymbol{p}_3 - \boldsymbol{p}_1 = \begin{bmatrix} -l_0\cos\frac{\alpha_1}{2}\sin\alpha_2 \\ -l_0\sin\frac{\alpha_1}{2}\sin\alpha_2 \\ -l_0\cos\alpha_2 \end{bmatrix} \tag{26}$$

Besides, BH and FG are symmetric about the *y*-*A*-*z* plane, then we have

$$\cos(\angle DAI) = \frac{(\overrightarrow{AD})_y}{|\overrightarrow{AD}|} = -\frac{\sqrt{2}\cos\frac{\alpha_1}{2}\cos\alpha_2\sin\alpha_2}{|\sin\alpha_2|\left|\cos\frac{\alpha_1}{2}\right|\sqrt{2\cos^2\frac{\alpha_1}{2}\cos^2\alpha_2 - 2\cos^2\frac{\alpha_1}{2} + 2}} \tag{27}$$

where $\left(\overrightarrow{AD}\right)_y$ is the projection length of $\overrightarrow{AD}$ along the *y*-axis.

We can also calculate $|\overrightarrow{AD}|$ by the cosine law,

$$\cos(\pi - \angle DAI) = \frac{|\overrightarrow{AL}|^2 + |\overrightarrow{AD}|^2 - |\overrightarrow{LD}|^2}{2\cdot|\overrightarrow{AL}|\cdot|\overrightarrow{AD}|} \tag{28}$$

where

$$|\overrightarrow{AL}| = |\overrightarrow{AB}|\cos\frac{\alpha_1}{2} = l_0\cos\frac{\alpha_1}{2}$$

$$|\overrightarrow{LD}| = |\overrightarrow{IL}| = \sqrt{|\overrightarrow{BI}|^2 - \left(\frac{1}{2}|\overrightarrow{BF}|\right)^2} = \sqrt{(2l_0)^2 - \left(l_0\sin\frac{\alpha_1}{2}\right)^2}$$

Combining Eqs. (27) and (28) and considering the length cannot be negative, $|\overrightarrow{AD}|$ can be derived as

$$|\overrightarrow{AD}| = \frac{l_0\sqrt{\cos\alpha_1 - 4\sin^2\alpha_2 - 4\cos\alpha_1\sin^2\alpha_2 + 7}}{\sqrt{2 - \cos\alpha_1\sin^2\alpha_2 - \sin^2\alpha_2}} + \frac{l_0\sin(2\alpha_2)(\cos\alpha_1 + 1)}{2|\sin\alpha_2|\sqrt{2\cos^2\alpha_2 + 2\cos\alpha_1\cos^2\alpha_2 + \sin^2\alpha_1\sin^2\alpha_2}} \tag{29}$$

Then we have

$$\overrightarrow{AD} = |\overrightarrow{AD}|\frac{\overrightarrow{BH}\times\overrightarrow{FG}}{|\overrightarrow{BH}\times\overrightarrow{FG}|} = \begin{bmatrix} 0 \\ -\frac{\sigma_1\cos\frac{\alpha_1}{2}\sin(2\alpha_2)}{\sigma_2} \\ \frac{\sigma_1\sin\alpha_1\sin^2\alpha_2}{\sigma_2} \end{bmatrix} \tag{30}$$

where

$$\sigma_1 = \frac{l_0\sqrt{\cos\alpha_1 - 4\sin^2\alpha_2 - 4\cos\alpha_1\sin^2\alpha_2 + 7}}{\sqrt{2 - \cos\alpha_1\sin^2\alpha_2 - \sin^2\alpha_2}} + \frac{l_0\sin(2\alpha_2)(\cos\alpha_1 + 1)}{2\sigma_3|\sin\alpha_2|}$$

$$\sigma_2 = \sigma_3|\sin\alpha_2|$$

$$\sigma_3 = \sqrt{2\cos^2\alpha_2 + 2\cos\alpha_1\cos^2\alpha_2 + \sin^2\alpha_1\sin^2\alpha_2}$$

Besides, $\overrightarrow{BD} = \overrightarrow{AD} - \overrightarrow{AB}$, so θ_{21} can be derived as

$$\theta_{21} = \arccos\left(\frac{\overrightarrow{BD}\cdot\left(-\overrightarrow{AB}\right)}{|\overrightarrow{BD}|\cdot\left|-\overrightarrow{AB}\right|}\right) = \arccos\left(\frac{\sqrt{2}\left(\cos\frac{\alpha_1}{2}\left(\cos\frac{\alpha_1}{2} - \frac{\cos\frac{\alpha_1}{2}\sin(2\alpha_2)\left(\frac{\sigma_1}{\sigma_2} + \sigma_4\right)}{\sigma_3}\right) - \frac{\cos\alpha_2}{2} + \frac{1}{2}\right)}{\sqrt{2\left(\cos\frac{\alpha_1}{2} - \frac{\cos\frac{\alpha_1}{2}\sin(2\alpha_2)\left(\frac{\sigma_1}{\sigma_2} + \sigma_4\right)}{\sigma_3}\right)^2 - \cos\alpha_1}\sqrt{+\frac{2\sin^2\alpha_1\sin^2\alpha_2\left(\frac{\sigma_1}{\sigma_2} + \frac{\sin(2\alpha_2)(\cos\alpha_1 + 1)}{2\sigma_3}\right)^2}{\sigma_5} + 1}}\right) \tag{31}$$

where

$$\sigma_1 = \sqrt{\cos\alpha_1 - 4\sin^2\alpha_2 - 4\cos\alpha_1\sin^2\alpha_2 + 7}$$

$$\sigma_2 = \sqrt{2 - \cos\alpha_1\sin^2\alpha_2 - \sin^2\alpha_2}$$

$$\sigma_3 = |\sin\alpha_2|\sqrt{\sigma_5}$$

$$\sigma_4 = \frac{\sin(2\alpha_2)(\cos\alpha_1 + 1)}{2|\sin\alpha_2|\sqrt{\sigma_5}}$$

$$\sigma_5 = 2\cos^2\alpha_2 + 2\cos\alpha_1\cos^2\alpha_2 + \sin^2\alpha_1\sin^2\alpha_2$$

To calculate θ_{22}, we need to know the lengths of three sides in the triangle $\triangle NKJ$. First, we have

$$\overrightarrow{AN} = \overrightarrow{AH} + \frac{1}{2}\overrightarrow{BD} = \begin{bmatrix} \frac{l_0\left(\sin\frac{\alpha_1}{2} - 2\cos\frac{\alpha_1}{2}\sin\alpha_2\right)}{2} \\ -\frac{l_0\cos\frac{\alpha_1}{2}}{2} - l_0\sin\frac{\alpha_1}{2}\sin\alpha_2 - \frac{\sigma_1\cos\frac{\alpha_1}{2}\sin(2\alpha_2)}{2\sigma_2} \\ \frac{\sigma_1\sin\alpha_1\sin^2\alpha_2}{2\sigma_2} - l_0\cos\alpha_2 \end{bmatrix} \tag{32}$$

where

$$\sigma_1 = \frac{l_0\sqrt{\cos\alpha_1 - 4\sin^2\alpha_2 - 4\cos\alpha_1\sin^2\alpha_2 + 7}}{\sqrt{2 - \cos\alpha_1\sin^2\alpha_2 - \sin^2\alpha_2}} + \frac{l_0\sin(2\alpha_2)(\cos\alpha_1 + 1)}{2\sigma_3|\sin\alpha_2|}$$

$$\sigma_2 = \sigma_3|\sin\alpha_2|$$

$$\sigma_3 = \sqrt{2\cos^2\alpha_2 + 2\cos\alpha_1\cos^2\alpha_2 + \sin^2\alpha_1\sin^2\alpha_2}$$

Since $\overrightarrow{AN}$ and $\overrightarrow{AK}$ are symmetric about the *y*-*A*-*z* plane, we have

$$|\overrightarrow{NK}| = |\overrightarrow{AK} - \overrightarrow{AN}| = l_0\left|\sin\frac{\alpha_1}{2} - 2\cos\frac{\alpha_1}{2}\sin\alpha_2\right| \tag{33}$$

According to the cosine law in $\triangle NKJ$, we have

$$\cos\theta_{22} = \frac{|\overrightarrow{JN}|^2 + |\overrightarrow{JK}|^2 - |\overrightarrow{NK}|^2}{2\cdot|\overrightarrow{JN}|\cdot|\overrightarrow{JK}|} \tag{34}$$

where $|\overrightarrow{JN}| = |\overrightarrow{JK}| = l_0$, further

$$\theta_{22} = \pi - \arccos\left(\frac{\left(\sin\frac{\alpha_1}{2} - 2\cos\frac{\alpha_1}{2}\sin\alpha_2\right)^2}{2} - 1\right) \tag{35}$$

Therefore, Eqs. (7), (13), (19), (20), (22), (23), (24), (31) and (35) form the whole kinematic equation set of two triangular

prisms with altered vertices, which shows that the group has two independent inputs indicating 2 DoF.

IV. Compatibility Analysis of the Altered Auxetic Metamaterial

A pair of double triangular prism groups as the one shown in Fig. 6(b) compose the metamaterial as shown in Fig. 9. Denoting the two prism groups of the whole structure as S^L and S^R, the compatible conditions of the whole structure are that the size lengths of the two groups are equal and

$$\theta_1^L = \theta_2^R, \theta_2^L = \theta_1^R \tag{36}$$

where θ_1^L and θ_2^L are defined as the assembly angles.

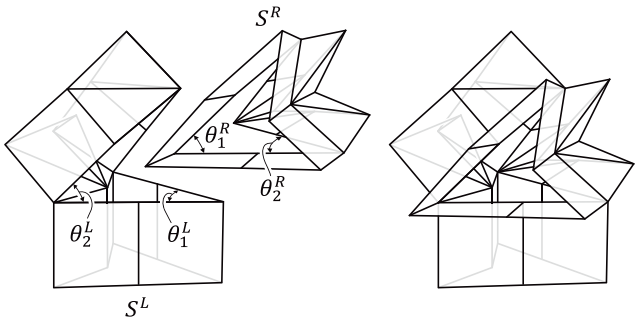

Figure 9. The two groups in exploded and assembled views.

The relationship between the folding angles α_1^L and α_2^L, and the assembly angles θ_1^L and θ_2^L are presented in Fig. 10. Once the folding angles α_1^L and α_2^L are given, the assembly angle θ_1^L, which equals to θ_{13}, can be calculated using Eq. (22) by replacing α_1 with α_1^L.

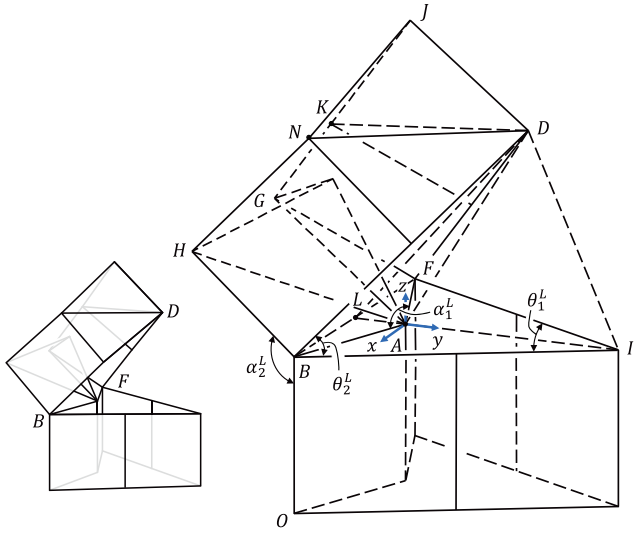

Figure 10. Relationship between the configuration angles and assembly angles.

To derive the assembly angle θ_2^L, we need to figure out the vectors $\overrightarrow{BD}$ and $\overrightarrow{BI}$ first. For $\overrightarrow{BD}$, we have

$$\overrightarrow{BD} = \begin{bmatrix} -l_0 \sin\frac{\alpha_1^L}{2} \\ l_0 \cos\frac{\alpha_1^L}{2} - \frac{\sigma_1 \cos\frac{\alpha_1^L}{2} \sin(2\alpha_2^L)}{\sigma_2} \\ \frac{\sigma_1 \sin\alpha_1^L \sin^2\alpha_2^L}{\sigma_2} \end{bmatrix} \tag{37}$$

where

$$\sigma_1 = \frac{l_0\sqrt{\cos\alpha_1^L - 4\sin^2\alpha_2^L - 4\cos\alpha_1^L\sin^2\alpha_2^L + 7}}{\sqrt{2 - \cos\alpha_1^L\sin^2\alpha_2^L - \sin^2\alpha_2^L}} + \frac{l_0 \sin(2\alpha_2^L)(\cos\alpha_1^L + 1)}{2\sigma_3|\sin\alpha_2^L|}$$

$$\sigma_2 = \sigma_3|\sin\alpha_2^L|$$

$$\sigma_3 = \sqrt{2\cos^2\alpha_2^L + 2\cos\alpha_1^L\cos^2\alpha_2^L + \sin^2\alpha_1^L\sin^2\alpha_2^L}$$

$\overrightarrow{BI}$ can be derived as

$$\overrightarrow{BI} = \overrightarrow{AI} - \overrightarrow{AB} = \left|\overrightarrow{AI}\right| \cdot [0,1,0]^T - \boldsymbol{p}_1 = \begin{bmatrix} -l_0 \sin\frac{\alpha_1^L}{2} \\ \frac{\sqrt{2}\, l_0\sqrt{\cos\alpha_1^L + 7}}{2} \\ 0 \end{bmatrix} \tag{38}$$

So we have

$$\cos\theta_2^L = \frac{\overrightarrow{BD}\cdot\overrightarrow{BI}}{|\overrightarrow{BD}|\cdot|\overrightarrow{BI}|} \tag{39}$$

Further

$$\theta_2^L = \arccos\left(\frac{\sqrt{2}\left(\sqrt{2}\,\sigma_1\sqrt{\cos\alpha_1^L + 7} - \cos\alpha_1^L + 1\right)}{2\,{\sigma_1}^2 - \cos\alpha_1^L} \Bigg/ \sqrt{4\left(\frac{2\sin^2\alpha_1^L\sin^2\alpha_2^L\left(\sigma_2 + \frac{\sin(2\alpha_2^L)(\cos\alpha_1^L + 1)}{2\sigma_3}\right)^2}{\sigma_4} + 1\right)} \right) \tag{40}$$

where

$$\sigma_1 = \cos\frac{\alpha_1^L}{2} - \frac{\cos\frac{\alpha_1^L}{2}\sin(2\alpha_2^L)\left(\sigma_2 + \frac{\sin(2\alpha_2^L)(\cos\alpha_1^L + 1)}{2|\sin\alpha_2^L|\sqrt{\sigma_4}}\right)}{\sigma_3}$$

$$\sigma_2 = \frac{\sqrt{\cos\alpha_1^L - 4\sin^2\alpha_2^L - 4\cos\alpha_1^L\sin^2\alpha_2^L + 7}}{\sqrt{2 - \cos\alpha_1^L\sin^2\alpha_2^L - \sin^2\alpha_2^L}}$$

$$\sigma_3 = |\sin\alpha_2^L|\sqrt{\sigma_4}$$

$$\sigma_4 = 2\cos^2\alpha_2^L + 2\cos\alpha_1^L\cos^2\alpha_2^L + \sin^2\alpha_1^L\sin^2\alpha_2^L$$

Once the compatible conditions in Eq. (36) are satisfied, the whole metamaterial can conduct a rigid folding. The altered auxetic model is presented in Fig. 11 with its motion process demonstrated in Fig. 12. It can be found that the whole structure squeezes in all directions, indicating the auxetic property of the unit cell with a negative Poisson's ratio.

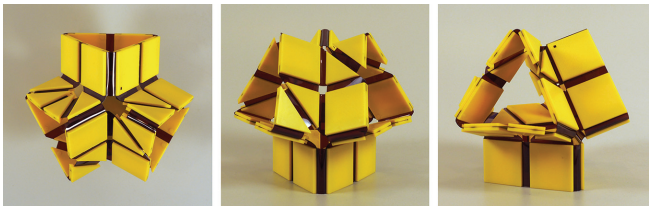

Top view Front view Right-side view

Figure 11. Orthographic views of the altered auxetic metamaterial.

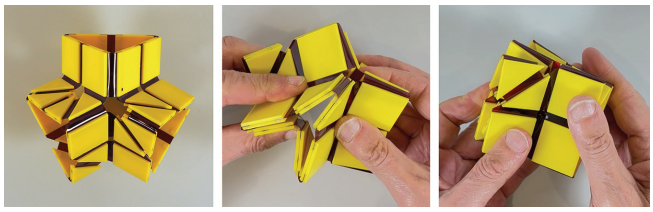

Figure 12. Rigid folding process of the altered auxetic metamaterial.

V. Conclusion

In this paper, we conducted the rigid foldability analysis of a transformable, flat-foldable shape – designed in 1996 by the Italian topology researcher Giorgio Scarpa – through the kinematic analysis of its vertices. It is found that the design, consisting of a prismatic tetrahedron with additional bisecting hinges on the walls of the extruded prisms, is not rigidly foldable. The flat folding occurs due to the deformation along the creases of the model. Eight additional diagonal creases were added to the model to create an altered auxetic metamaterial, with two pairs of symmetric creases added to the central vertices and two pairs added to the corner vertices. The altered model was proved to be rigidly foldable with detailed kinematic modeling and compatibility analysis. The altered metamaterial, while introducing the rigid foldability, preserved the flat-foldability, the load-bearing capacity, and the auxetic property. The basic unit model can be tessellated to form large-scale metamaterials with high load-bearing capacity and ease of storage and transportation, which has great potential applications in lightweight sheltering, sustainable furniture and building substrates. The thickness of the plates needs to be accommodated by the creases in further applications.

Acknowledgment

P.T. is grateful to his teacher and mentor Giorgio Scarpa, whose 1996 original design of two transformable shapes – *figure trasformabili* – based on the cube and the tetrahedron, inspired this work. Thanks to Oda De Sisti Scarpa who generously made Scarpa's archive available for research. Thanks to Prof. Paul Breedveld, Department of BioMechanical Engineering, and Prof. Just Herder, Department of Precision and Microsystems Engineering, sponsors of my 2017–2018 visiting scholar appointment in the Faculty of Mechanical Engineering at Delft University of Technology (TU Delft), the Netherlands, where this work was first started. Thanks to Johannes Overvelde, Soft Robotic Matter, AMOLF, Amsterdam, whose design of prismatic metamaterials suggested the value of Scarpa's unpublished designs, and Agustin Iniguez Rabago, for sharing their materials and ideas. Thanks to Elizabeth Montano and Jojo Minnick, Industrial Design students at San Francisco State University, for help with the construction of the physical models. Thanks to the anonymous reviewers who provided many valuable comments and suggestions, which helped to greatly improve the manuscript. Many thanks to Prof. Huijuan Feng and Wujie Shi for enthusiastically diving into the analysis and modeling of Scarpa's transformable figure, and to Prof. Jian Dai for his continued support and mentoring since the 4th ReMAR conference held in Delft, the Netherlands, in 2018.

References

[1] X. Hu, T. Tan, B. Wang and Z. Yan, "A reprogrammable mechanical metamaterial with origami functional-group transformation and ring reconfiguration", *Nature Commun.*, vol. 14, p. 6709, 2023.

[2] A. Jamalimehr, M. Mirzajanzadeh, A. Akbarzadeh and D. Pasini, "Rigidly flat-foldable class of lockable origami-inspired metamaterials with topological stiff states", *Nature Commun.*, vol. 13, p. 1816, 2022.

[3] K. Liu, P.P. Pratapa, D. Misseroni, T. Tachi and G.H. Paulino, "Triclinic Metamaterials by Tristable Origami with Reprogrammable Frustration" *Adv. Mater.*, vol. 34, p. 2270298, 2022.

[4] B. Li, J.L. Silverberg, A.A. Evans, C.D. Santangelo, R.J. Lang, T.C. Hull and I. Cohen, "Topological kinematics of origami metamaterials". *Nature Phys*, vol. 14, pp. 811–815, 2018.

[5] J.L. Silverberg, A.A. Evans, L. McLeod, R.C. Hayward, T. Hull, C.D. Santangelo and I. Cohen, "Using origami design principles to fold reprogrammable mechanical metamaterials", *Science*, vol. 345, no. 6197, pp. 647-650, 2014.

[6] E.T. Filipov, T. Tachi and G.H. Paulino, "Origami tubes assembled into stiff, yet reconfigurable structures and metamaterials", *Proc. Natl. Acad. Sci. U.S.A.*, vol. 112, no. 40, pp. 12321-12326, 2015.

[7] H. Fang, S.C. A. Chu, Y. Xia and K.W. Wang, "Programmable self-locking origami mechanical metamaterials", *Adv. Mater.*, vol. 30, no. 15, p. 1706311, 2018.

[8] T. Frenze, M. Kadi and M. Wegener, "Three-dimensional mechanical metamaterials with a twist", *Science*, vol. 358, no. 6366, pp. 1072-1074, 2017.

[9] Z. Wang, C. Luan, G. Liao, J. Liu, X. Yao and J. Fu, "Progress in auxetic mechanical metamaterials: structures, characteristics, manufacturing methods, and applications", *Advanced Engineering Materials*, vol. 22, no. 10, p. 2000312, 2020.

[10] S. Tomita, K. Shimanuki, S. Oyama, H. Nishigaki, T. Nakagawa, M. Tsutsui, Y. Emura, M. Chino, H. Tanaka, Y. Itou and K. Umemoto, "Transition of deformation modes from bending to auxetic compression in origami-based metamaterials for head protection from impact", *Scientific Report*, vol.13, p. 12221, 2023.

[11] S. Kamrava, D. Mousanezhad, H. Ebrahimi, R. Ghosh and A. Vaziri, "Origami-based cellular metamaterial with auxetic, bistable, and self-locking properties", *Scientific Report*, vol.7, p. 46046, 2017.

[12] A. Wickeler and H. Naguib, "Novel origami-inspired metamaterials: Design, mechanical testing and finite element modelling", *Materials & Design*, vol.186, p. 108242, 2020.

[13] W. Wu and Z. You, "Modelling rigid origami with quaternions and dual quaternions", *Proc. Math. Phys. Eng. Sci.*, vol. 466, no. 2119, pp. 2155–2174, 2010.

[14] J. Cai, Y. Zhang, Y. Xu, Y. Zhou and J. Feng, "The foldability of cylindrical foldable structures based on rigid origami", *J. Mech. Des.*, vol. 138, no. 3, p. 031401, 2016.

[15] J.S. Dai and J.R. Jones, "Mobility in metamorphic mechanisms of foldable/erectable kinds", *J. Mech. Des.*, vol. 121, no. 3, pp. 375–382, 1999.

[16] J.S. Dai and J.R. Jones, "Kinematics and mobility analysis of carton folds in packing manipulation based on the mechanism equivalent", *Proc. Inst. Mech. Eng. C: J. Mech. Eng. Sci.*, vol. 216, no. 10, pp. 959–970, 2002.

[17] J.S. Dai and J.R. Jones, "Matrix representation of topological changes in metamorphic mechanisms", *J. Mech. Des.*, vol. 127, pp. 837–840, 2005.

[18] Y. Zhang, Y. Gu, Y. Chen, M. Li, X. Zhang, "One-dof rigid and flat-foldable origami polyhedrons with slits", *Acta Mechanica Solida Sinica*, vol. 36, pp. 479–490, 2023.

[19] T. Tachi, "Generalization of rigid-foldable quadrilateral-mesh origami", *J. Int. Assoc. Shell Spatial Struct.*, vol. 50, no. 3, pp. 173–179, 2009.

[20] H. Feng, R. Peng, J. Ma and Y. Chen, "Rigid foldability of generalized triangle twist origami pattern and its derived 6R linkages", *Journal of Mechanisms and Robotics-Transactions of the ASME*, vol. 10, no. 5, p. 051003, 2018.

[21] J. Cai, Y. Zhang, Y. Xu, Y. Zhou and J. Feng, "The foldability of cylindrical foldable structures based on rigid origami", *J. Mech. Des.*, vol. 138, no. 3, p. 031401, 2016.
[22] J. Ma, H. Feng, Y. Chen, D. Hou and Z. You, "Folding of tubular waterbomb", *Research*, vol. 2020, p. 1735081, 2020.
[23] H. Feng, J. Ma, Y. Chen and Z. You, "Twist of tubular mechanical metamaterials based on waterbomb origami", *Scientific Reports*, vol. 8, no.1, p. 9522, 2018.
[24] P.Trogu. Giorgio Scarpa: Italian designer, bionics and topology researcher, teacher, and artist. https://res.trogu.com/scarpa/ Accessed Feb. 20, 2024.
[25] G. Scarpa. *Models of Rotational Geometry*. Trans. P. Trogu (draft) of Italian Edition: *Modelli di Geometria Rotatoria*, Zanichelli, 1978. https://res.trogu.com/scarpa/pdf/scarpa_models_geometry_122pp.pdf
[26] G. Scarpa, *Bionic Models*. Trans. P. Trogu (draft) of Italian Edition: *Modelli di bionica*, Zanichelli 1985. https://res.trogu.com/scarpa/pdf/bionic_models_complete.pdf
[27] P. Trogu. Giorgio Scarpa's Model of a Sea Urchin Inspires New Instrumentation. *Leonardo* 2019; 52 (2): 146–151. doi: https://doi.org/10.1162/leon_a_01384
[28] P. Trogu, Bio-inspired models of rotational geometry. Seminar presentation. Department of BioMechanical Engineering, Delft University of Technology (TU Delft), The Netherlands. December 21, 2017, p. 101. https://res.trogu.com/scarpa/pdf/tu_delft_3me_trogu_scarpa_2017-12-21.pdf
[29] J. Overvelde, J. Weaver, C. Hoberman and K. Bertoldi, "Rational design of reconfigurable prismatic architected materials", *Nature*, vol. 541, pp. 347–352, 2017. https://www.nature.com/articles/nature20824
[30] P.R. Cromwell, *Polyhedra*, Cambridge University Press, 79 (1999).
[31] H. Zhang, J. Wu, Y. Zhang and D. Fang, "Multistable mechanical metamaterials: A brief review", *Trans. Nanjing Univ. Aeronaut. Astronaut.*, vol. 38, no. 1, pp. 1-17, 2021.
[32] A. Iniguez-Rabago, Y. Li and J.T.B. Overvelde, "Exploring multistability in prismatic metamaterials through local actuation". *Nat Commun*, vol. 10, no. 1, p. 5577, 2019. https://doi.org/10.1038/s41467-019-13319-7
[33] K. Xiao, X. Zhou and J. Ju, "Effect of disconnection of deformable units on the mobility and stiffness of 3D prismatic modular origami structures using angular kinematics", *Sci. Rep.*, vol. 11, p. 18259, 2021.
[34] H. Feng, R. Peng, S. Zang, J. Ma and Y. Chen, "Rigid foldability and mountain-valley crease assignments of square-twist origami pattern", *Mech Mach Theory*, Vol. 152, p. 103947, 2020.
[35] R.S. Hartenberg and J. Denavit, *Kinematic synthesis of linkages*, McGraw-Hill, 1964.